

Multi-scale Colorectal Tumour Segmentation Using a Novel Coarse to Fine Strategy

Kun Zhang^{1,2,3}
zhangkun_nt@163.com

Danny Crookes³
d.crookes@qub.ac.uk

Jim Diamond⁴
Jim.Diamond@pathxl.com

Minrui Fei¹
mrfei@staff.shu.edu.cn

Jianguo Wu²
wu.jg@ntu.edu.cn

Peijian Zhang²
zhang.pj@ntu.edu.cn

Huiyu Zhou³
h.zhou@ecit.qub.ac.uk

¹ School of Mechatronic Engineering and Automaton, Shanghai University, China

² School of Electrical Engineering, Nantong University, China

³ ECIT, Queen's University Belfast, Belfast, UK

⁴ PathXL Ltd., Northern Ireland Science Park, Belfast, BT3 9DT, UK

Abstract

This paper addresses the problem of colorectal tumour segmentation in complex real world imagery. For efficient segmentation, a multi-scale strategy is developed for extracting the potentially cancerous region of interest (ROI) based on colour histograms while searching for the best texture resolution. To achieve better segmentation accuracy, we apply a novel bag-of-visual-words method based on rotation invariant raw statistical features and random projection based l_2 -norm sparse representation to classify tumour areas in histopathology images. Experimental results on 20 real world digital slides demonstrate that the proposed algorithm results in better recognition accuracy than several state of the art segmentation techniques.

1 Introduction

Colorectal cancer is the third most common form of cancer worldwide, and the second highest cause of death from cancer in the UK [1, 2]. The most accurate diagnosis of colorectal cancer is based on the interpretation of the features extracted from whole colorectal histopathological slides. Diagnostic decisions are generally made by a pathologist and the process can be subjective and extremely tedious. Digital pathology is the management and interpretation of pathological information from digital microscopic images. Compared to traditional pathology, a major advantage of digital pathology is that slides can also be analysed using software rather than just manual analysis which depends on many years' experience [3, 10]. Consequently, many researchers have begun to develop

computer aided diagnosis methods by applying computer vision techniques to identify the spatial extent and location of tumours in diseases such as breast cancer [4], prostate cancer [5], lung cancer [6], and colorectal cancer [7] on digitized tissue sections.

Even so, in many digital processing cases, the chosen method may not perform satisfactorily. In general, there are two challenges in automatic detection of tumours in histopathological images. One of them is the enormous volume of data which the algorithms have to cope with. Compared with radiological and other imaging modalities, for instance, a typical whole colorectal histological slide, which has a tissue area of 30 mm by 20 mm, is scanned to give an image of $120,000 \times 80,000$ pixels, or 27 GB of uncompressed colour image data. An example of a digital slide can be seen in Fig. 1. The second challenge is that, on the one hand, tumours in histopathology slides usually differ in colour, shape, and texture; while on the other hand, cancerous tissue can look similar to noncancerous tissue.

In this paper, we choose to use a coarse-to-fine approach for efficient tumour segmentation, for two reasons. Firstly, although an enormous volume of literature has been dedicated to image segmentation, there is little consensus on the comparison of experimental results with those of pathologists. Secondly, in a whole slide image, irrelevant tissue types significantly disturb state of the art classification methods [20, 21, 19, 18, 38, 39]. For instance, at the feature extraction stage, since different tissue types have different morphologies, some of the state of the art methods are not rotation invariant, while other approaches which are rotation invariant sacrifice raw pixels precision [39]. If we can eliminate irrelevant tissue types, it is much easier for later tumour classification.

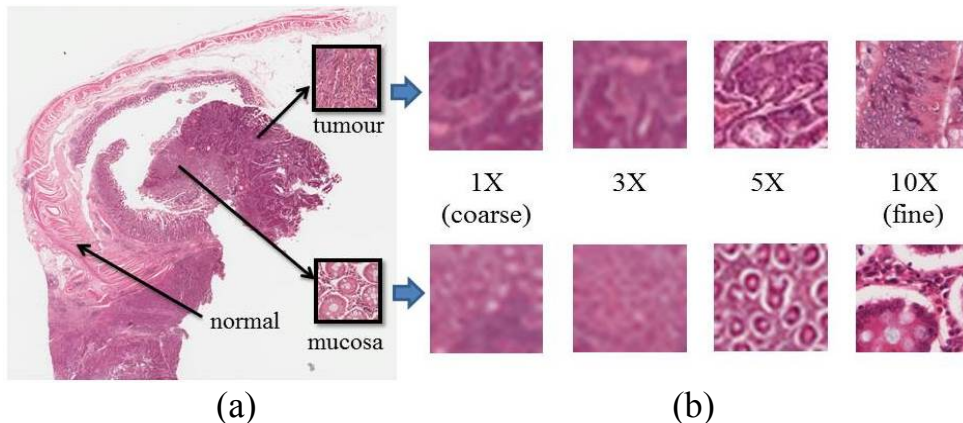


Figure 1: Example of a digital slide: (a) Digital slide of size 97349×73293 . (b) Zoomed-in view of sub-regions at various resolutions. Best viewed in colour.

At a low resolution, a pathologist usually spots a possible tumour region using global features such as colour and shape to analyse the properties of the region of interest. Here we attempt to simulate the procedure of a pathologist. We propose to extract the ROI by applying a colour model and morphological operations to the original image. The ROI is then optimized using Euclidean distance based histograms in order to reduce the noisy margin. Afterwards, to be able to perform tumour segmentation at the best resolution, we deploy a Convergence Index (CI) approach to detect nuclei by fitting circles. At the tumour classification stage when the resolution is at a high level, we use a rotation invariant feature and random projection based l_2 -norm sparse representation technique for more accurate segmentation. The main contributions of our work include: 1) we propose a multi-scale strategy for tumour segmentation, which simulates the decision making of a pathologist from the coarse-to-fine processing. 2) A novel Rotation Invariant Raw Statistics (RIRS) feature and random projection based l_2 -norm sparse representation method is developed for making the tumour classification process more effective.

The paper is structured as follows. Section 2 presents related work on automatic tumour segmentation. Section 3 introduces a novel framework for colorectal tumour segmentation. Experimental results using the proposed method are presented in section 4. Finally, we provide concluding remarks and perspectives for future work in section 5.

2 Related work

Early global tumour segmentation approaches reported in the literature include region based and boundary based methods. Colour models based on saliency detection are usually used for region detection. Yang [8] introduced a robust colour-based segmentation algorithm for histological structures, which used gradients in the colour space to handle the issues of stain variability. Sun [30] used Mahalanobis distance to classify tissues into four types of colour features. The use of colour saliency can be restricted by the background formation and may cause the loss of spatial information of the features. Instead, in this paper, we propose an adaptive ROI extraction algorithm using Euclidean distance combined with a RGB colour model to refine the ROI.

Boundary detection is typically used as a category-specific cue. Subbanna [9] used Markov Random Field (MRF) for brain tumour segmentation. The main advantage of their approach is that the MRF corrects the local mischaracterizations of tissues that typically occur due to noise, inhomogeneity and normalization problems. Zhang [31] presented a customized boundary encoding method to tackle the issue of over-segmentation, leading to small regions. Chen [35] proposed a deformable model to improve segmentation of complex structures. However, these boundary based methods still face some challenges in the histopathology segmentation process because the boundaries of tumour tissue can be mixed with other normal tissue types such as mucosa. Inspired by pathology research, we deploy a boundary based method to consider the number of nuclei as a local feature indicator of the best image resolution for tumour classification. To our knowledge, this is the first time nuclei numbers have been used to determine image resolutions.

Recently, people have started using local structure based feature classification methods for tumour segmentation. Bag of Words (BoW) methods are one of the powerful tools for extracting higher dimensional features for image classification. Yoshimuta [12] explored a local feature recognition method using BoW to detect colorectal cancer. The issue of using BoW is the computational cost. For instance, it took a standard computer over 8 seconds to encode an image patch of size 200×200 [18], while a full image has over 5,000 patches. Random projection has attracted the attention of the community due to its performance in dimensionality reduction. Zhang [13] firstly used 3D regions for colorectal polyp detection using random projection, and the results showed that the invasive cancer was discriminated with approximately 87% accuracy. This shows that it is promising to investigate random projection for tumour classification.

Alternatively, researchers have suggested multi-scale frameworks for tumour segmentation. For example, Wang [11] deployed a multi-resolution method for the diagnosis of cervical intraepithelial neoplasia. The tumour tissue was firstly segmented at a low (2X) resolution, and the boundaries were further fine-tuned at a higher (20X) resolution. Liu [32] exploited a novel shape descriptor with multi-scale diffusion response. However, these multi-scale systems used the same resolution at each stage, and could not adapt to different images in the same database. Our approach is capable of being adaptive to different resolutions and hence achieves better segmentation results.

3 Proposed algorithm

As mentioned in the first section, the proposed framework for automatic colorectal tumour segmentation begins with RGB colour segmentation at low resolutions. This is followed by applying histogram distance measurement to detect the refined microstructure of the ROI boundary. Then we deploy a convergence index method to detect the shape of nuclei by counting the number of whole nuclei at different resolutions, and then use this number as an indicator of the best image resolution for tumour classification. The rotation invariant feature and random projection based l_2 -norm sparse representation is dynamically optimised for classification. Detailed descriptions now follow.

3.1 Adaptive ROI extraction

Most of the area in a whole histopathology slide usually contains background clutter and normal tissue. We segment these regions using a simple but effective method. Colour is the most perceptual factor to the human visual system [36] especially for pathologists. An RGB colour model is an operator that allows contrasting regions to be detected, and can provide more intuitive histogram information than other common models such as CMY, HSI, and L^*a^*b et al. To achieve this result, two histograms are created, one for the Red histogram and the other for Blue histogram in RGB domain. This is because Red and Blue components significantly correspond to the stained tumour tissues. Afterwards, we generate a number of points and regions which can be separated using mean values to get an initial region of interest (see Fig. 2(b)). A morphological Close operation extends the boundaries of the foreground to improve the initial ROI region (see Fig. 2(c)). Euclidean distance is a popular measure of the similarity between two images [33]. It is used as a criterion for refining the ROI extraction at an adaptive resolution (see Fig. 2(d)). To reduce processing time and memory requirements, 3x is set as the final resolution for the ROI extraction.

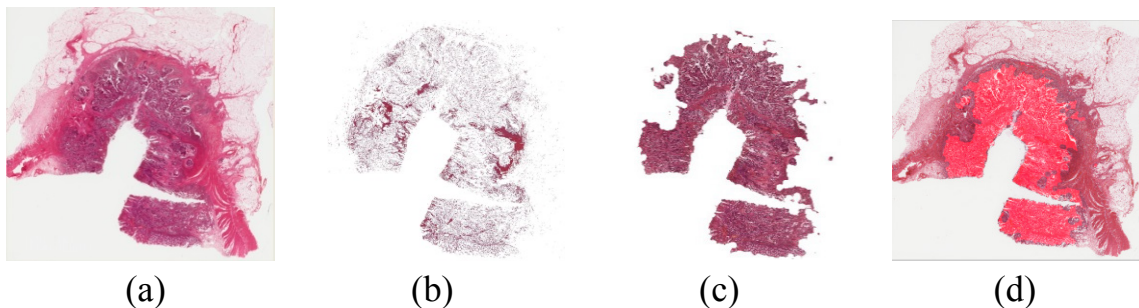


Figure 2: ROI extraction step by step: (a) original image, (b) result after R and B threshold, (c) result after morphology, and (d) refined ROI overlaid on the original image.

3.2 Dense nuclei detection using convergence index

Given the extracted ROI, where the majority of tumour tissue may (or may not) have been detected, we now zoom in order to segment the ROI area further because mucosa tissue has similar colour features to those of tumour. Normal tissue is usually associated with sparse and dispersive nuclei, while proliferation nuclei usually appear in tumour tissue. Pathologists note that, nuclei clustering and growth have a close relationship with tumour detection. Based on this, we wish to count the number of complete nuclei which can indicate the best image resolution for tumour classification. The best resolution is

determined by counting nuclei at each resolution, and finding the resolution where the number stabilizes.

Most nuclei detection approaches assume that nuclei are mostly isolated in a brighter region with less clutter [15, 25, 26, 34]. However, in our case, nuclei appear often in groups and in dark regions filled with background noise. In addition, the nucleus border is fused with the background. See Fig. 3(a). Our approach to nuclei detection is based on a Convergence Index (CI) [14], which is much more efficient than other nuclei detection methods because CI works in a gradient field [37], and just obtains the most noticeable information. It begins by using a gradient vector to obtain margin information as shown in Fig. 3(b), and the maximization weight of the CI creates the spatial nucleus coordinates which form a gradient map shown in Fig. 3(c). Fig. 3(d) shows the corresponding accumulation array in 3D. To reduce the influence of noise, we calculate the colour value of the centre position in this way: If the intensity value is over a certain threshold (in this project the threshold is 0.7, determined experimentally, we set it as a noisy point. Fig. 3(e) is the final result of the nuclei detection. The aim of this algorithm is to detect the nucleus's shape by accumulating the number of complete nuclei in a block. A few incomplete nuclei near the block border are missing, but this will not affect selecting the best resolution if the number of nuclei larger than a threshold of 80 nuclei.

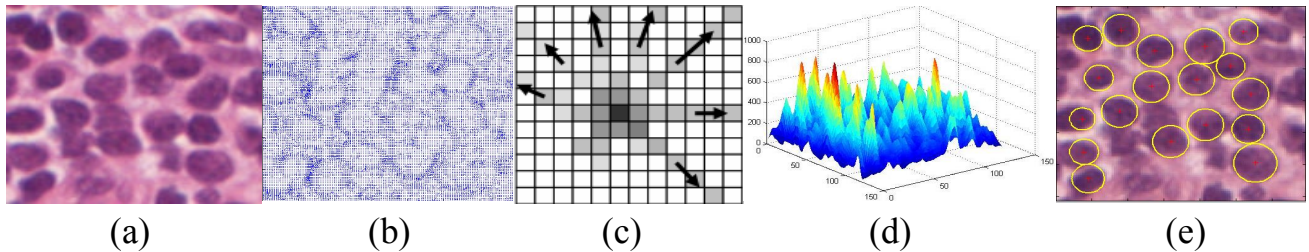


Figure 3: Nuclei detection using convergence index: (a) Original nuclei image, (b) gradient field of the nuclei, (c) weight distribution of CI, (d) suspected nuclei accumulation array in 3D, the peaks are the suspected nuclei, (e) result of nuclei detection. Best viewed in colour.

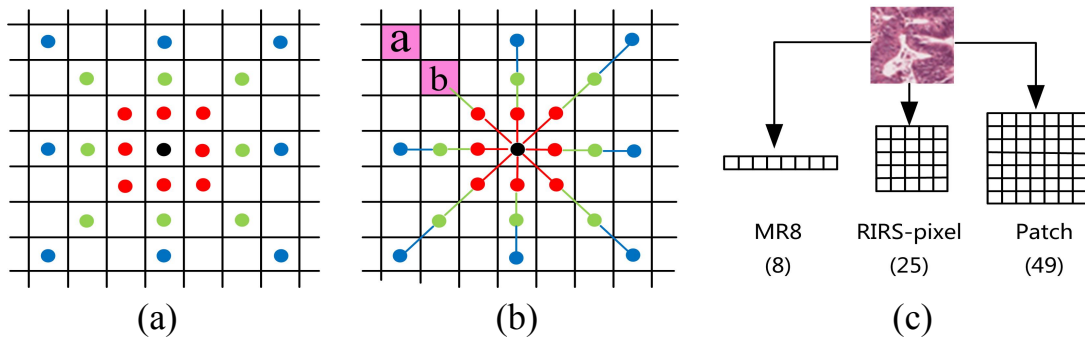


Figure 4: Rotation Invariant Raw Statistics feature: (a) RISR-pixel feature, (b) RISR-radial diff feature, (c) feature dimension based on three features. Best viewed in colour.

3.3 Tumour classification using RIRS feature and random projection based l_2 -norm sparse representation

In recent years, the BoW model has shown promise for complex classification [27, 28]. It uses local features to form textons, for example MR8 filter [19] and Patch feature [38], and to encode a histogram representing the frequency of the repetition of the textons over the global image statistically. However, rotation invariance and texton clustering accuracy are barriers to its application.

In this paper, we propose a Rotation Invariant Raw Statistics feature (RIRS) for tumour feature selection, and the motivation of the new feature is as follows. Firstly, a

histopathological image may not demonstrate any structured direction. Secondly, the state of the art features such as MR8, Patch, LBP, PR [16] and SPR [39] have certain disadvantages in medical applications. For example, Patch features are not rotation invariant; most SPR features are interpolation points which are calculated from the neighbouring raw features. A RIRS feature is based on a Patch feature. We choose the raw pixels from 4 target orientations. Fig. 4(a) shows RIRS-pixel features; the selected points are formed into a RIRS-pixel feature vector. We also use the inter-scale information to deploy the RIRS-radial diff feature, as shown in Fig. 4(b). Radial diff feature means the absolute difference value of 2 pixels from the same orientation and neighbouring scales. For example, in Fig. 4(b), the absolute difference of pixels “a” and “b” is one feature from RIRS-radial diff feature. In Fig. 4(c) it is easy to find out that based on a 7 by 7 image, a RIRS feature is not only rotation invariant but also has fewer feature dimensions. The RIRS-pixel and RIRS-radial diff features can be calculated by:

$$x^{pixel} = [x_{0,0}, (x_{1,1}, x_{1,2}, x_{1,3}, x_{1,4}), \dots, (x_{8,1}, x_{8,2}, x_{8,3}, x_{8,4})]^T \quad (1)$$

$$x^{rad} = [(x_{1,0} - x_{0,0}, x_{1,2} - x_{0,0}, x_{1,3} - x_{0,0}, x_{1,4} - x_{0,0}), \dots, (x_{8,1} - x_{7,1}, x_{8,2} - x_{7,2}, x_{8,3} - x_{7,3}, x_{8,4} - x_{7,4})]^T \quad (2)$$

where $x_{i,j}$ is a pixel with different scales and orientations. i means scale and j means orientation.

It is hard to capture the dominant pathological feature in a medical image. However, the state of the art BoW methods still use K-means to form the texton dictionary and encode histogram features. It has been proven that K-means is easy and fast to implement but can only work in the compressed domain and the representation accuracy is limited because only the cluster centre is used to approximate the samples [18]. In this paper we use l_2 -norm sparse representation to form textons and code histogram features. We use l_2 -norm, instead of K-means, to characterize the texton dictionary and encode histogram features based on the following reasons: First, since the training dictionary is an offline process, it is not necessary to force the encoding coefficients to be sparse just for efficiency reasons. Second, the dominant pathological feature is not easy to classify, and l_2 -norm regularization is good enough to yield a stable solution to the dictionary and coding histogram coefficients. In addition, it has been proven that Random Projection (RP) is a computationally simple and information preserving technique to reduce a high dimensional space to a lower dimensional one [16]. It is natural to fuse RP with l_2 -norm based coding histogram coefficients. The l_2 -norm based texton learning model is proposed by:

$$\min_{D, \alpha} (\|x - DK\|_2^2 + \lambda \|K\|_2^2 + \eta \sum_{i=1}^n \|\alpha_i - \delta\|_2^2) \quad s. t. \quad d_j^T d_j = 1 \quad (3)$$

where $D = [d_1, d_2, \dots, d_j], d_k \in R^m$ is the texton learning model, $K = [\alpha_1, \alpha_2, \dots, \alpha_l]$ are coding coefficients, δ is the mean of all α_i without distortion. i.e., $\delta = 1/n \sum_{i=1}^n \alpha_i$ when distortion does not appear, $\delta = 1/(n-u) (\sum_{i=1}^n \alpha_i - \sum_{f=1}^u \alpha_f)$, u is the number of distortion. α_f is distortion which is 50% upper or downer than mean value.

The RP based coding histogram coefficients approach is to build a sparse feature vector, and RP can be used to avoid the shortcomings of other dimensionality reduction approaches such as principle component analysis (PCA) [24]. For instance, PCA cannot guarantee that the image is well preserved after dimensionality reduction. Random

projection theory has a strong theoretical basis supported by the Johnson-Lindenstrauss lemma [17]. That is, for any two images, x_1 and $x_2 \in \mathbb{R}^m$, if sparse space $d \geq O(\log m / \varepsilon^2)$, and $0 < \varepsilon < 1$, the distance between them is preserved:

$$1 - \varepsilon \leq \frac{\|\phi(x_1 - x_2)\|_2}{\|x_1 - x_2\|_2} \leq 1 + \varepsilon \quad (4)$$

RP addresses the compressed sensing problem. The high-dimensional space has an intrinsic dimensionality that is much lower than the original dimensional space; therefore, RP is able to extract texton features without information loss. Within the framework of RP based coding histogram coefficients in Fig. 5, for each feature vector of the image, we can use RP to produce a compact and sparse representation, where only the entries corresponding to the same textons will have non-zero values, while the other entries in a compact vector are zeros. Then we can form the histogram coefficient as a new feature.

Fig. 6 shows two colorectal patches of different classes and their 400 dimension histogram features. We can see that the histogram features of different classes are very different. For instance, in the upper two histograms, the features around “50”, “100” and “350” show strong differences and it is convenient for the later classification. At the same time, when texton number changes, the two histograms for the same image patch also show a sufficient difference. The upper histograms are built from 7 textons and the lower histograms are constructed from 33 textons, and it is clear that the similarity of the two histograms based on 33 texton is much lower than 7 textons based histograms, and it is easy to find more discriminating features for classification.

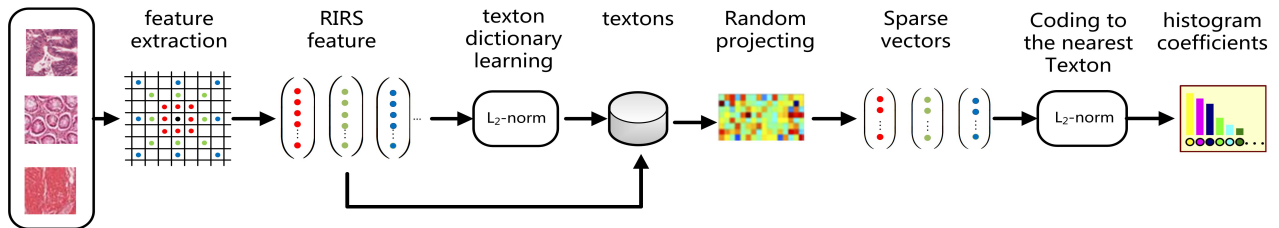


Figure 5: l_2 -norm based texton dictionary learning and Random projection based coding histogram coefficients process. Best viewed in colour.

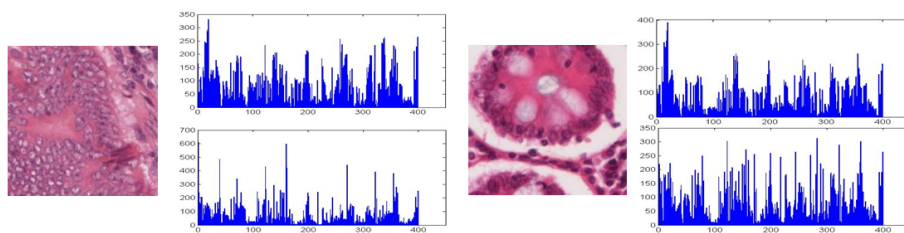


Figure 6: Tumour and mucosa images and their encoding histogram features (upper histogram – 7 textons and lower histogram – 33 textons). Best viewed in colour.

4 Experimental results

To demonstrate the operation of the proposed method, we perform three sets of experiments on ROI extraction, nuclei detection, and malignant tumour classification, and then report the results of all the related methods where applicable. Databases are described in section 4.1, followed by the results and analysis in section 4.2.

4.1 Databases

A total of 20 Hematoxylin and eosin stained whole colorectal cancer digital slides were supplied by a local company and used as the basis for training and testing. These digital slides each have a size around $100,000 \times 150,000$. Each slide was examined by pathologists and each region was annotated to be one of two major classes: tumour and normal. These annotated slides were used as the ground truth for the training and testing.

For malignant tumour identification, the slides are divided into small blocks for training and testing. Each individual block is assigned to one of four categories: Stroma (including all fibromuscular tissue, tumour and mucosa (in both transverse and longitudinal variants) (Fig. 7). Each block needs to be large enough to demonstrate the characteristics of a particular tissue type. For this reason, image blocks were initially chosen to be 200×200 pixels at adaptive magnification (more details can be found in Section 3.2). In total, we use 500 blocks per category, giving a total of 2,000 blocks. In addition, we also use a public texture database “KTH_TIPS” [23] to validate our proposed method. In our experiments, we treat it as a separate database.

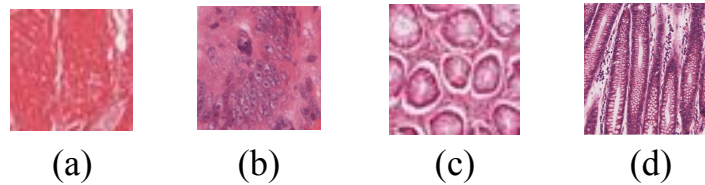


Figure 7: Four categories of colorectal images: (a) Stroma, (b) tumour, (c) Mucosa(Transverse), and (d) Mucosa(Longitudinal).

4.2 Experimental results and analysis

ROI extraction is demonstrated step by step, from initial to refined segmentation, in Fig. 8. The contribution of histogram distance measurement starts from Fig. 8(c); when it satisfies a certain criterion, the algorithm will move to the next resolution of the image. Red blocks are the optimized areas, compared with the initial and refined results.

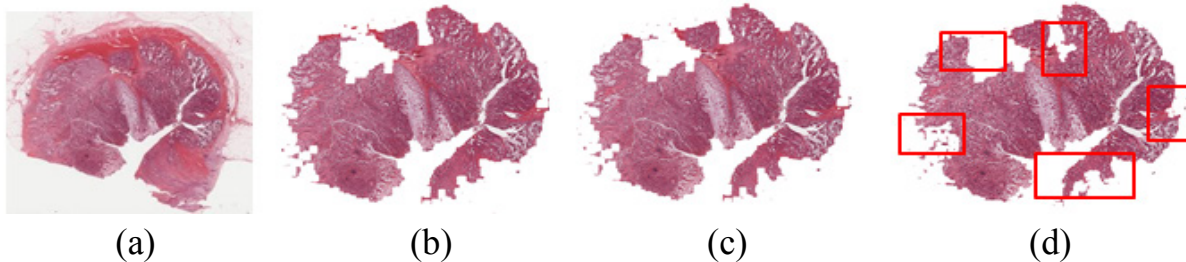


Figure 8: ROI extraction from initial to refined segmentation: (a) original image, (b) initial ROI, 1st segmentation at 1X resolution, (c) 2nd segmentation at 1X resolution, histogram distance: 0.968, and (d) refined ROI. 5th segmentation at 3X resolution, histogram distance: 0.9988. Best viewed in colour.

Fig. 9 shows the nuclei detection using the proposed CI method at different resolutions. We can see that the nuclei detection gets easier as we move to higher resolutions. From these images, 12 images at 8X are chosen for the best resolution, 8 images at 10X are chosen for the best resolution.

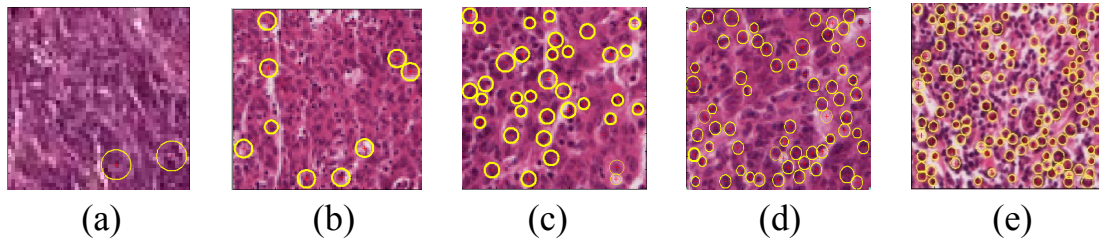


Figure 9: Nuclei detection using the proposed Hough transform method at different resolutions: (a) 1X resolution, (b) 2X resolution, (c) 4X resolution, (d) 6X resolution, and (e) 8X resolution. Best viewed in colour.

There are two key parameters in our malignant tumour classification experiments: 1) The RP dimensionality m and 2) the number of textons L per class. Parameter m controls the sparsity of coding coefficients in the texton encoding. We discover from the experiments that when m is small, the classification accuracy increases rapidly; however, when m reaches one third of the texton dimensionality, the classification accuracy is stable. Parameter L is the number of textons per class used in the dictionary, which controls the capacity of the dictionary to represent the texture appearance. We conducted a series of experiments with different numbers of textons on the texture datasets. The more samples are used, the higher accuracy is achieved.

For our main database, 50 PR dimensions and 70 textons per class are employed. On the KTH TIPS database, 10 PR dimensions and 40 textons per class were used. All the experiments were performed in the Matlab programming environment on a laptop with a 2.10 GHz Intel processor and 4GB memory.

We used the standard random forest [40] as the classifier to classify the results and then compared our method with recently published texture classification methods [20, 21, 19, 18, 38, 39] (see Table 1). When there are enough training samples, most of the methods can achieve good classification accuracy for the public KTH_TIPS database. The proposed method works well and is only slightly worse than SRP for this database. GLCM suffers the impact of texture difference and produces the lowest accuracy. However, the upper and lower accuracy in our main colorectal pathology database indicates that these colorectal pathology images are very difficult to classify. The proposed method achieves the best result on this database, and SRP is in the third place. This may be because SRP uses interpolation to achieve rotation invariance; however, interpolation in a high resolution medical image will make the K-means more difficult for texton learning and feature coding.

Methods	KTH_TIPS	colorectal pathology slide
ELBP [20]	91.5%	77.5%
GLCM [21]	71.5%	63.8%
MR8 [19]	92.6%	86.2%
TEISF [18]	97.1%	91.5%
Patch [38]	93.1%	91.9%
SRP [39]	98.3%	91.8%
RIRS-pixel	97.5%	91.9%
RIRS- radial diff	97.7%	92.2%

Table 1: Classification rates by different methods.

Finally, we compare the segmentation results of the proposed algorithm against those by pathologists. Examples are shown in Fig. 10, where the green line is the ground truth and

the second row shows the results of our method. Root mean squared error (R_{MSE}) [22] is a quantitative performance indicator and can be used to evaluate the system performance. The average R_{MSE} is 0.0935, the maximum R_{MSE} is 0.151, and the minimum R_{MSE} is 0.052.

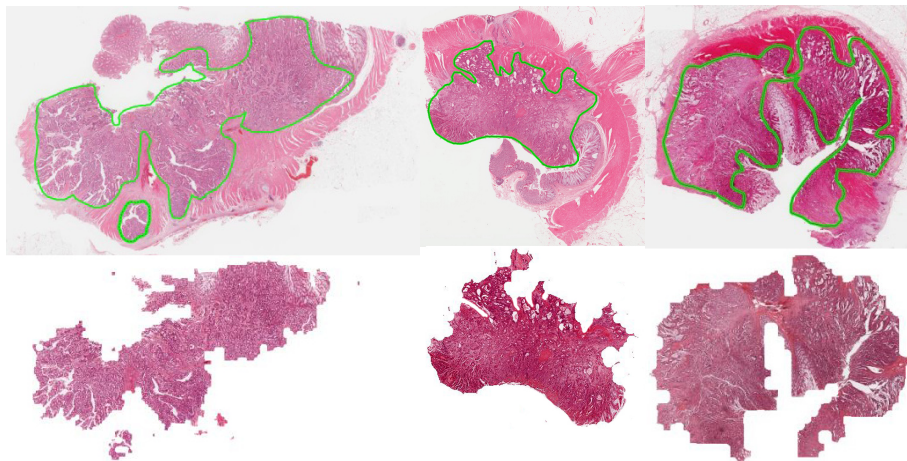


Figure 10: Final results compared with ground truth and RMES evaluation: row 1- ground truth, row 2- segmentation using the proposed method. Best viewed in colour.

5 Conclusions and future work

In this paper we have introduced an efficient multi-scale approach for pathological colorectal tumour segmentation. Our method applied a RGB colour model and histogram distance for refining the ROI extraction. To find the best resolution adaptively, we used convergence index to generate some gradient vectors to obtain nucleus's margin information. We deployed RIRS features and random projection based l_2 -norm sparse representation to balance the classification accuracy. Experimental results show that this new approach has better performance than other state of the art techniques in terms of recognition accuracy on a database of 20 whole digital slides. In the future, we intend to combine a global texture model with our approach. The motivation for this is to further reduce the computation cost of the classification.

Acknowledgements

This research is supported by the China Scholarship Council (CSC) under grant agreement no 201406890060, and this research is supported by Key Project of Science and Technology Commission of Shanghai Municipality under Grant No. 14JC1402200.

References

- [1] J. Ferlay, H.R. Shin, F. Bray, and D. Forman. Cancer incidence and mortality worldwide. International Agency for Research on Cancer. <http://globocan.iarc.fr>, 2010.
- [2] Cancer research UK. Cancer stats incidence. <http://www.cancerresearchuk.org>, 2014.
- [3] M.N. Gurcan, L.E. Boucheron, and A. Madabhushi. Histopathological image analysis: A review. *IEEE Trans Biomed Eng.*, 2:147–171, 2009.
- [4] M. Veta, J. P. Pluim, J. Paul, and A. M. Viergever. Breast Cancer Histopathology Image Analysis: A Review. *IEEE Trans. Biomed Eng.*, 61(5), 1400-1411, 2014.
- [5] S. Naik, S. Doyle, and S. Agner. Automated gland and nuclei segmentation for grading of prostate and breast cancer histopathology. In *Proc. of ISBI*, 284-287, 2008.

- [6] J.C. Sieren, J. Weydert, and A. Bell. An automated segmentation approach for highlighting the histological complexity of human lung cancer. *Annals of Biomed Eng.* 38(12):3581-3591, 2013.
- [7] W.Q. Li, J.G. Zhang, S. McKenna, M. Coats, and F. Carey. Classification of colorectal polyp regions in optical projection tomography, In *Proc. of ISBI*, 736-739, 2013.
- [8] L. Yang, P. Meer, and D. Foran. Unsupervised segmentation based on robust estimation and color active contour models. *IEEE Trans. Inf. Technol. Biomed.*, 9(3): 475–486, 2005.
- [9] N. Subbanna, D. Precup, and T. Arbel. Iterative multilevel MRF leveraging context and voxel information for brain tumour segmentation in MRI. In *Proc. of CVPR*, 2014.
- [10] S. Parisot, H. Duffau, S. Chemouny, and N. Paragios. Graph-based detection, segmentation & characterization of brain tumours. In *Proc. of CVPR*, 2012.
- [11] Y.H. Wang, D. Crookes, O.S. Eldin, S.L. Wang, P. Hamilton, and J. Diamond. Assisted diagnosis of cervical intraepithelial neoplasia (CIN). *IEEE J. Sel. Topics Signal Process.* 3(1), 112-121, 2009.
- [12] J.Yoshimuta, M. Kawakami, B. Raytchev, K. Kaneda, S. Yoshida, Y. Takemura, K. Onji, R. Miyaki, and S. Tanaka. Computer-aided colorectal tumour classification in NBI endoscopy using local features. *Med Image Anal.* 17(1):78-100, 2013.
- [13] W.Q. Li, M. Coats, and J.G. Zhang. Comparative analysis of feature extraction methods for colorectal polyp images in optical projection tomography. In *Proc. of MIUA*, 2013.
- [14] P. Quelhas, M. Marcuzzo, A.M. Mendonça, M.J. Oliveira, and A. Campilho. Cancer cell detection and invasion depth estimation in brightfield images. In *Proc. of BMVC*, 2009.
- [15] H. Irshad, A. Veillard, L. Roux, and D. Racoceanu. Methods for Nuclei Detection, Segmentation, and Classification in Digital Histopathology: A Review—Current Status and Future Potential. *IEEE Rev Biomed Eng.* 7:97-114, 2014.
- [16] L. Liu and P. Fieguth. Texture classification from random features. *IEEE Trans. Pattern Anal. Machine Intell.*, 34(3):574-586, 2012.
- [17] S. Dasgupta and A. Gupta, An elementary proof of a theorem of Johnson and Lindenstrauss. *Random Struct Algor*, 22(1):60-65, 2003.
- [18] J. Xie, L. Zhang, and J. You. Effective texture classification by texton encoding induced statistical features. *Pattern Recognition*, 48(2):447-457, 2015.
- [19] M. Varma, and A. Zisserman, A statistical approach to material classification from single images. *Int J Comput Vision.* 62(2):61-81. 2005.
- [20] T. Ojala, M. Pietikäinen, and T. Mäenpää. Multi-resolution gray-scale and rotation invariant texture classification with local binary patterns. *IEEE Trans. Pattern Anal. Machine Intell.*, 7(24):971-987. 2002.
- [21] A.Rampun, H. Strange, and R.Zwiggelaar. Texture segmentation using different orientations of GLCM features. In *Proc. of ACM*, 2013.
- [22] L. Liang, R. Xiao, F. Wen, and J. Sun. Face alignment via component-based discriminative search. In *Proc. of ECCV*, 2008.
- [23] E. Hayman, B. Caputo, M. Fritz, and J. O. Eklundh. On the significance of real-world conditions for material classification. In *Proc. of ECCV*, 2004.
- [24] T. Randen and J. Husøy. Filtering for texture classification: a comparative study. *IEEE Trans. Pattern Anal. Machine Intell.*, 21(4):291-310, 1999.
- [25] X. Chen, X. Zhou, and S. T. C. Wong. Automated segmentation, classification, and tracking of cancer cell nuclei in time-lapse microscopy. *IEEE Trans. Biomed Eng.* 53(4):762–766, 2006
- [26] A.A. Nawandhar, L. Yamujala, and N. Kumar. Image segmentation using thresholding for cell nuclei detection of colon tissue. In *Proc. of ICACCI*, 2015.
- [27] M. Varma and A. Zisserman. A statistical approach to material classification using image patches. *IEEE Trans. Pattern Anal. Machine Intell.*, 31(11): 2032-2047, 2009.

- [28] J. Zhang, M. Marszalek, S. Lazebnik, and C. Schmid. Local features and kernels for classification of texture and object categories: a comprehensive study, *Int'l J. of Computer Vision*, 73(2):213-238, 2007.
- [29] R.E. Fan, K.W Chang, C.J Hsieh, X.R Wang, and C.J. Lin. LIBLINEAR: A library for large linear classification. *Journal of Machine Learning Research*, 9:1871-1874, 2008.
- [30] Y.N. Sun, Y.Y. Wang, S.C. Chang, L.W. Wu, and S.T. Tsai. Color-based tumor tissue segmentation for the automated estimation of oral cancer parameters. *Microsc Res Tech*, 73(1):5-13, 2010.
- [31] D. Zhang, M.L. Xu, L. Quan, Y. Yang, Q.Q. Qin, and W.B. Zhu. Segmentation of tumour ultrasound image in HIFU therapy based on texture and boundary encoding, *Phys. Med. Biol*, 2015.
- [32] J.F. Liu, S.J. Wang, M.G.Linguraru, J.H. Yao, and R.M. Summers. Computer-aided detection of exophytic renal lesions on non-contrast CT images. *Medical Image Analysis*, 19(1):15-29, 2015.
- [33] L.Wang, Y. Zhang, and J. Feng. On the Euclidean distance of images. *IEEE Trans. Pattern Anal. Machine Intell.*, 27(8):1334-1339, 2005.
- [34] R. Ali, M. Gooding, T. Szilágyi, B. Vojnovic, M. Christlieb, and M. Brady. Automatic segmentation of adherent biological cell boundaries and nuclei from brightfield microscopy images. *Machine Vision and Applications*, 23(4):607-621, 2012.
- [35] T. Chen, and D. Metaxas. A hybrid framework for 3D medical image segmentation. *Med Image Anal*, 9(6):547-565, 2005.
- [36] J.V.D. Weijer, and T. Gevers. Boosting saliency in color image features. In *Proc. of CVPR*, 2005.
- [37] H. Kobatake, and S.Hashimoto. Convergence index filter for vector fields. *IEEE Trans. Image Processing*, 8(8):1029-1038, 1999.
- [38] M. Varma, and A. Zisserman. A statistical approach to texture classification from single images. *International Journal of Computer Vision*, 62(1-2):61-81, 2005.
- [39] L. Liu, P. Fieguth, D. Clausi. et al. Sorted random projections for robust rotation-invariant texture classification. *Pattern Recognition*, 45(6):2405-2418, 2012.
- [40] A. Cutler, D. R. Cutler, J. R. Stevens, Random Forests. *Machine Learning*, 45(1):157-176, 2011.